Transient thermal-electrical performance modelling of solar concentrating photovoltaic (CPV) receiver

Transient thermal-electrical performance modelling of solar concentrating photovoltaic (CPV) receiver

Ali O. M. Maka*, Tadhg S. O'Donovan

Institute of Mechanical, Process and Energy Engineering, School of Engineering and Physical Sciences
Heriot-Watt University, Edinburgh, EH14 4AS, United Kingdom
*Corresponding author: maca_4212@yahoo.co.uk

Abstract

The cell efficiency of a solar CPV system can be enhanced by the dissipation of the thermal load from the receiver assembly. The performance of the solar cell is influenced by the incident light and cell operating temperature. In this study, a triple-junction solar cell, under a concentration ratio of 500x and cell dynamic efficiency, is considered for a wide range of operating temperatures (25-80 ^{o}C). The key purpose of this work is to simulate both transient and steady-state operating conditions, based on the temperature-dependent conversion efficiency. In this study, a transient model has been developed using COMSOL Multiphysics®. A live-link technique of COMSOL with MATLAB® is used to couple of successive thermal and electrical steady-state models for a fixed timestep. The performance behaviour of electrical parameters J_{sc}, V_{oc}, P, FF and P_{max} are investigated. The results show that a dynamical efficiency, compared with constant efficiency and integrated error, was approximately 12%. The cell cycle steady-state temperature occurs at a maximum cell temperature of 78.4 ^{o}C within 30s at the convective heat transfer coefficient h_{conv}= 1400 W/m^2 K and 500x of concentration ratio. Thus, steady-state cell temperature and time to reach it significantly dependence on the values of the environmental parameters of DNI, AM and T_{amb}. Therefore, we can determine the thermal response of h_{conv} to keep the value of $T_{cell} \leq 80$ ^{o}C.

Keyword: Transient model; Steady-state condition; Conversion efficiency; Cell temperature; Concentrating photovoltaic receiver.

1. Introduction

There has been a rapid increase in global energy demand, which has given the energy sector more motivation and has increased the attraction for investors, to study and development of renewable energy resources (Council, 2016; REGR, 2018). Currently, Photovoltaics (PV) solar energy technology is deemed to be one of the cleanest, most plentiful and least costly in contrast to other renewable energy sources. Therefore, that greatly encouraged scientists and

researchers to develop CPV as a renewable energy technology solution (AEO, 2019; Watts, 2013).

High-efficiency multi-junction solar cells are widely used in Concentrating Photovoltaic (CPV) systems; due to their high conversion efficiency, a reduction in the cell area of semiconductor materials, and utilising the low cost of concentrating materials (Philipps et al., 2015; Philipps and Bett, 2014). The evolution of multi-junction solar cells has been largely developed in both factories and laboratories. From this, the efficiency of such as solar cells has been reported about 46% (Geisz et al., 2017; Green et al., 2019). CPV technology relies on the output power increasing solar flux. Usually, CPV systems consist of a receiver assembly, focusing optic and tracker, it's operating with various ranges of concentration ratios (Sweet et al., 2018; Talavera et al., 2015). Efficient heat dissipation of HCPV is the challenge to ensure optimal performance in real environmental conditions. Hence, the heat source on the receiver assembly comes from the cells as a result of light concentration, which leads to high cell temperatures (Cotal et al., 2009; Kinsey and Edmondson, 2009).

As a result of CPV, the solar flux heats the top surface of the solar cells; therefore, the accumulation of thermal energy raises the temperature of the surface of the solar cells. In turn, this leads to a reduction of the cell conversion efficiency; this can also have a negative effect on the long-term operation of the cell, leading to mechanical failures (Kumar et al., 2012; Maka and O'Donovan, 2020). Considering the performance behaviour under a concentration ratio of 500x, if the PV module is insulated, then the temperature can reach a value in excess of 1400 ^{o}C. Therefore, it is important to understand and investigate the effects of cell temperature (T_{cell}) on triple-junction solar cell electrical performance parameters (Araki et al., 2002; Zhangbo et al., 2009).

High temperatures cause a reduction in conversion efficiency as each subcell of a multi-junction cell is connected in series. This results in a major debilitating effect on the maximum power and open circuit's voltage (Cotal and Sherif, 2006). In CPV systems, it's important to predict the solar cell's temperature, which can then be used in performance analysis and characterisation. Hence, to keep a high level of performance efficiency, heat needs to be effectively dissipated from the cell to the environment (Muron et al., 2011; Theristis and O'Donovan, 2015).

The majority of electronic devices operate over a long period, and their mechanisms of cooling are designed for steady-state operation conditions. Nevertheless, in some electronic

devices, applications do not ever operate long enough to achieve steady-state operation. In these cases, it might be adequate to employ a restricted cooling procedure, such as thermal storage, for a short time (buffering), or not to use one at all (Cengel, 1998).

Wang *et al.* performed a study of an HCPV module based on implementing a forward voltage technique to measure and monitor the time-varying nature of a junction's temperature. A detailed analysis of the thermal characteristic of the Finite Element Method (FEM) model was established and compared with experimental data (Wang et al., 2010). Muller *et al.* had proposed thermal transient measurements based on the temperature coefficient for the heating and natural cooling of the CPV module. The measurement of V_{oc} from the cells was used to determine the cell operating temperature. Instrument sensors are utilised to measures both the back-plate temperature and the V_{oc} parameters. Consequently, the main advantage of this measurement technique is that the cell temperature has a very quick response to steady-state conditions (Muller et al., 2015).Torres-Lobera *et al.* simulated dynamic performance in a PV module system. This model was performed on the PV solar module's string, which comprised of six series-connected modules and analysed using MATLAB/ Simulink software. The module temperatures, *P–V* curves and maximum power points for the string/PV module were investigated. Lastly, the measurements of environmental parameters and the electrical parameters of the PV solar power plant were used for validation (Torres-Lobera and Valkealahti, 2014). Migliorini *et al.* investigated the performance of a thermal-electrical model of a PV solar module, that took into account dynamic performance behaviour. The thermal model considered five different featured layers and the electrical model considered the behaviour of five performance parameters. As a result, predictions of the electric power produced with both explicit and simple relations were reported. (Migliorini et al., 2017).

In CPV systems, cell efficiency is an important key parameter to be considered in performance characterisation (Cotal et al., 2009). However, the temperature dependence of the cell efficiency is to be taken into account in any modelling or design (Cotal et al., 2009; Nishioka et al., 2010). In this study, models for predicting the steady-state cell temperature of CPV at 500x have been developed, and also used to determine the transient thermal and electrical performance.

Despite the many studies related to dynamic models in estimating PV solar cell temperature, which has been introduced previously in literature; in this research, a developed model of CPV receiver for transient response is presented. The significance of the transient model is being the link between the ideal modelling and the environmental operating conditions. A

thermal model based on the steady-state equation is obtained by considering the total energy balance in the PV module; this builds upon the previous study model by 'Maka and Donovan' in the references (Maka et al., 2019a, b). Consequently, the current study expands in this area to consider the transient and steady-state operations. This study composed of five main sections and respectively presented. Section 1 summary of introduction; Section 2 summarised the methodology and the approaches that have been used. Section 3 describes the numerical modelling of the electrical model, thermal FEM model and receiver geometry and boundary conditions. Section 4 detailed the results and discussions; hence, temperature-dependent on cell efficiency, validation, heat power and thermal response analysis. Also, the effects of varying irradiance intensity on steady-state cell temperature, and the effects of varying ambient temperature in the steady-state cell temperature. Lastly, Section 5 draws the key conclusions and the suggestion for future work.

Nomenclature

A_c	Area of the cell (m^2)	**Greek symbols**	
A_s	Convective area (m^2)	η_{opt}	Optical efficiency
CR	Concentration Ratio (x)	σ	Stefan–Boltzmann constant ($W/(m^2K^4)$)
DNI	Direct Normal Irradiance (W/m^2)	ε	Surface emissivity (-)
G	Solar direct irradiance ($W/m^2/nm$)	η_c	Cell efficiency
h_{conv}	Convection heat transfer coefficient ($W/m^2 K$)	λ	wavelength (nm)
J_{sc}	Short circuit current density (A/m^2)	α	Material constant (eV/K)
J_o	Dark current density (A)	β	Material constant (K)
k_b	Boltzmann constant (eV/K)	β_η	Efficiency temperature coefficient
n	Diode ideality factor (-)	γ	Constant (-)
q	Electron charge (c)	K	Constant ($A/(cm^2K^4)$)
q_{heat}	Heat power (W)	**Abbreviations**	
R_s	Series resistance (Ω)	*AM*	Air Mass
SR	spectrum response (A/W)	GaInP	Gallium Indium Phosphide
∂T	Temperature different	GaInAs	Gallium Indium Arsenide
Δt	Time different (s)	Ge	Germanium
T_{amb}	Ambient temperature (^oC)	EQE	External Quantum Efficiency
T_o	Temperature at standard condition (^oC)	FEM	Finite Element Method
T_c	Cell temperature (^oC)	1D	One-dimensional
V_{oc}	Open circuit voltage (V)	3D	Three-dimensional
P	Power (*W*)	FF	Fill Factor
$P_{max.}$	Maximum power (*W*)	HCPV	High Concentrating Photovoltaic
T	Time (s)	DBC	Direct Bonded Copper
		Al_2O_3	Aluminium Oxide

2. Methodology

Fig.1 illustrates the flowchart diagram describing the modelling approach. The electrical model consists of a GaInP/GaInAs/Ge, triple-junction cell, with a standard *DNI* = 1000 W/m^2 and at CR = 500x, which is detailed in Section 3.1. Temperature dependence has been predicted for cell efficiency and heat power generation from incident solar power. The modelling results are compared with a commercial CPV cell for temperature range 25-80 ^{o}C.

The numerical simulation of the three-dimensional study with a thermal model is coupled with an electrical model, which is detailed in Section 3.2. The model was developed using MATLAB live-link to couple the characteristics of the changing materials of the model for each convergent and transient step. Initial cell temperature is modified after each iteration, changing both the electrical conversion efficiency and the rate of heat transfer from the cell. Steady-state is deemed to have been achieved when the cell temperature remains constant with subsequent iterations, indicating the conservation of energy has been satiated.

A transient model is a model that contains dependent variables that changes over time and is used here to determine the effect of a changing environment on the performance of a HCPV cell. Besides, this is known as a dynamic model, time-dependent model or unsteady model (Multiphysics, 2012). The model proposed here is a sequence of several steady-state conditions, where the initial condition of the iterative solution is the final steady-state condition of the previous timestep, as shown in Fig.1.

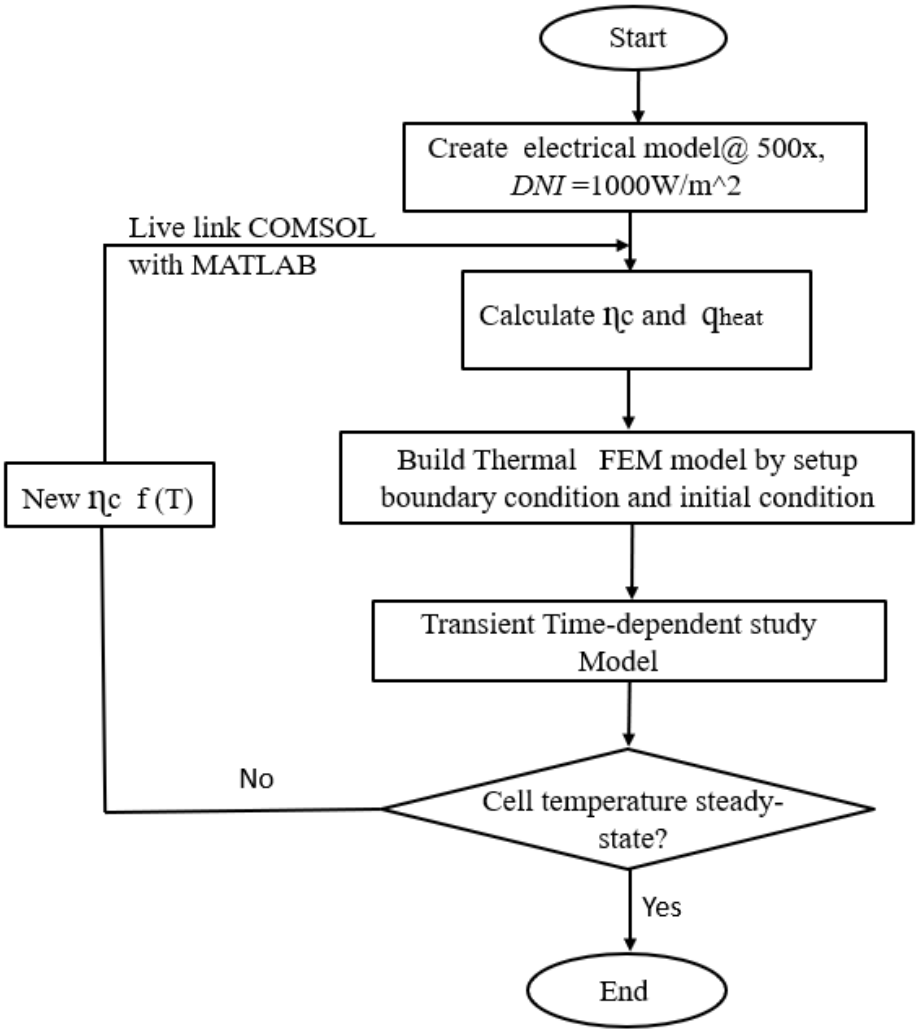

Fig.1. Flowchart of the modelling process.

3. Numerical modelling

3.1. Electrical model of triple-junction cells

The electrical model is the cornerstone of performance evaluation and energy generation of PV solar cells. A solar cell is a semiconductor material based on *p-n* junctions, designed to produce current by absorbing the light of energy photons. Performance evaluation of solar cells is dependent on parameters of voltage-current characteristics. Triple-junction solar cells are made of III-V materials; it consists of three subcell's, GaInP/GaInAs/Ge, monolithically stacked. It is important to determine the short current density generated by the cells, as given by Eq. (1) (Peharz et al., 2009).

$$J_{sc,i} = CR.\int_{\lambda 1}^{\lambda 2} SR_{i(\lambda)}.\eta_{opt(\lambda)}.G_{(\lambda)}.d\lambda \quad (1)$$

Where *CR* is a concentration ratio of 500x, and *SR* is the spectral response and η_{opt} is the optic efficiency. Equation (2) (known as the Shockley diode equation) characterises the current produced by the solar cell:

$$J_{,i} = J_{ph,i} - J_{0,i}\left(\exp\frac{q(V_{,i} + J.R_{s,i})}{n.K_b.T_c} - 1\right) - \frac{V_{,i} + J.R_{s,i}}{R_{sh}} \quad (2)$$

Where R_s is series resistance, V is the voltage, R_{sh} is the shunt resistance, J_{ph} is the photocurrent. In the ideal case, the photocurrent is equal to short circuit density $J_{ph} = J_{sc}$. The R_{sh} is of a magnitude that can be neglected (Theristis and O'Donovan, 2015). The overall current is determined by the light-induced current from the diode dark current and is given by Eq. (3). The total current of the three subcells, in series connection, is limited by lower current density and the total voltage will be the sum of three subcells. The open-circuit voltage (V_{oc}) can be given by the relationship (4):

$$J_{,i} = J_{o,i}\left(\exp\frac{q(V + J_{,i}.R_s}{n.K_b.T_c} - 1\right) - J_{sc,i} \quad (3)$$

$$V_{oc,i} = \frac{n.K_b.T_c}{q}\ln\left(\frac{J_{sc,i}}{J_{0,i}} + 1\right) \quad (4)$$

Where n is the diode ideality factor, K_b is Boltzmann constant, T_c is temperature, q is the electron charge, R_s is a series resistance, and J_o is the reverse saturation current. The voltage output of the entire cell is the sum of the three subcells. The total current is determined by limiting the lowest photocurrent generated by three subcells. The Fill Factor (*FF*) is the ratio of the maximum output power, P_{max}, from the solar cell, divided by the open circuit voltage and short-circuits current density, as given in Eq. (5):

$$FF = \frac{P_{max}}{V_{oc}.J_{sc}} = \frac{J_{max}.V_{max}}{V_{oc}.J_{sc}} \quad (5)$$

The electrical efficiency of the cell (η_{el}) is quantified by dividing power output by power input as given by Eq.(6). Where P_{out} is a delivered power and P_{in} is the amount of incident power in the solar cell.

$$\eta_{el} = \frac{P_{max}}{P_{in}} = \frac{J_{sc}.V_{oc}.FF}{p_{in}} \quad (6)$$

Cell efficiency η_c, as a function of temperature, can be calculated by Eq.(7) (Ceylan et al., 2016; Sarhaddi et al., 2010). Where η_{el} is cell electrical efficiency for the concentration ratio, β_η is efficiency temperature coefficient, and T_o is reference condition temperature.

$$\eta_{c(T)} = \eta_{el}\left[1 - \beta_\eta (T_c^* - T_o)\right] \quad (7)$$

3.2. Thermal FEM model

Thermal FEM modelling utilises COMSOL Multiphysics, which is iteratively solved by Partial Differential Equations (PDEs). In the FEM, the simulation starts by producing the geometry and dividing it into finite elements. The "Heat Transfer in Solids" simulation physics is used to develop 1D and 3D dynamic thermal models.

The aluminium oxide interlayer offers electrical insulation between the top and bottom subcell materials. The insulation materials in the middle of the Direct Bonded Copper (DBC) sandwich between the bottom and top copper, as Al_2O_3 has excellent combined properties as an electrical insulator and thermal conductor (García et al., 2016). To simplify the model, the electrical terminals and bypass-diodes are not considered.

For the optimum design of a CPV system from the perspective of conversion efficiency, the level of temperatures of a CPV system should be maintained as low as possible. Therefore, to implement a heat transfer model, it is essential to design a system which can investigate the variance in temperature and system performance. The thermal design is built on our understanding of the processes of heat transfer, from assembly to unit level, by conduction, convection and radiation. Eq.(8) (Aldossary et al., 2016; Theristis et al., 2012) expresses the heat dissipation by conduction through the receiver of the solid component. Where K is thermal conductivity, (∂T/∂x) is the temperature gradient, A is conductive area and q_{con} is conduction heat transfer (W/m^2).

$$q_{con} = -K.A.\frac{\partial T}{\partial x} \quad (8)$$

The amount of heat that is dissipated by convection from the surface to the air is expressed in Eq.(9) (Theristis et al., 2012). Where q_{conv} is convection heat transfer (W/m^2), A_s is convective area, h_{conv} is a convection heat transfer coefficient.

$$q_{conv} = h_{conv}.A_s.\frac{\partial T}{\partial x} \quad (9)$$

The heat loss by radiation transferring heat by electromagnetic waves to the environment is expressed by Eq.(10) (Theristis et al., 2012). q_{rad} is radiative heat flux (W/m^2), T_s is surface temperature, ε is surface emissivity, and σ is the Stefan-Boltzmann constant.

$$q_{rad} = \varepsilon.\sigma.A.(T_s^4 - T_{amb}^4) \quad (10)$$

Thermal equilibrium with the surrounding environment occurs in the electronic device when it is not under operating conditions and at the same temperature of the surrounding media. Although, when the device is active, the component's, and the solar cell device, the temperature begins to increase due to the absorption of heat, the temperature of the device stabilises at the point when the heat generated equals the heat released throughout the cooling mechanism. At that point, the device has reached steady-state operating conditions. The period during the warming-up, when the component temperature rises, is called the operational transient period (Cengel, 1998).

3.3. Receiver geometry and boundary condition

The boundary conditions in the solid domains are applied. The model geometry of a receiver assembly is attached to a Direct Bonded Copper (DBC) carrier, made of copper/Al_2O_3 ceramic/copper. The receiver configuration set at the bottom convective area is about $5.13x10^{-4}$ m^2, and the solar cell area is 1cm^2. Using the multi-junction solar cell's heat source at CR = 500x, the heat power is generated by the portion that is not converted to electricity. Heat transfer in the solid-state is due to the material's thermal properties. A convective heat transfer boundary condition has been applied to the backside of the plate, h_{conv} = 1400 W/m^2 K. The ambient temperature around the receiver was set to 25 ^{o}C. The optimum geometry mesh of normal size, free triangle type was applied. Fig.2 shows a 3D receiver structure, and the selected point at the centre of the cell for the 1D single plot. Table 1 listed the single CPV receiver assembly dimensions.

Table 1 Dimensions of CPV receiver assembly (Theristis and O'Donovan, 2015).

Receiver layer	Width (mm)	Thickness (mm)	Length (mm)
Solar cell	10	0.19	10
Copper	19.5	0.25	24
Al_2O_3	21	0.32	25.5
Copper	20.5	0.25	25

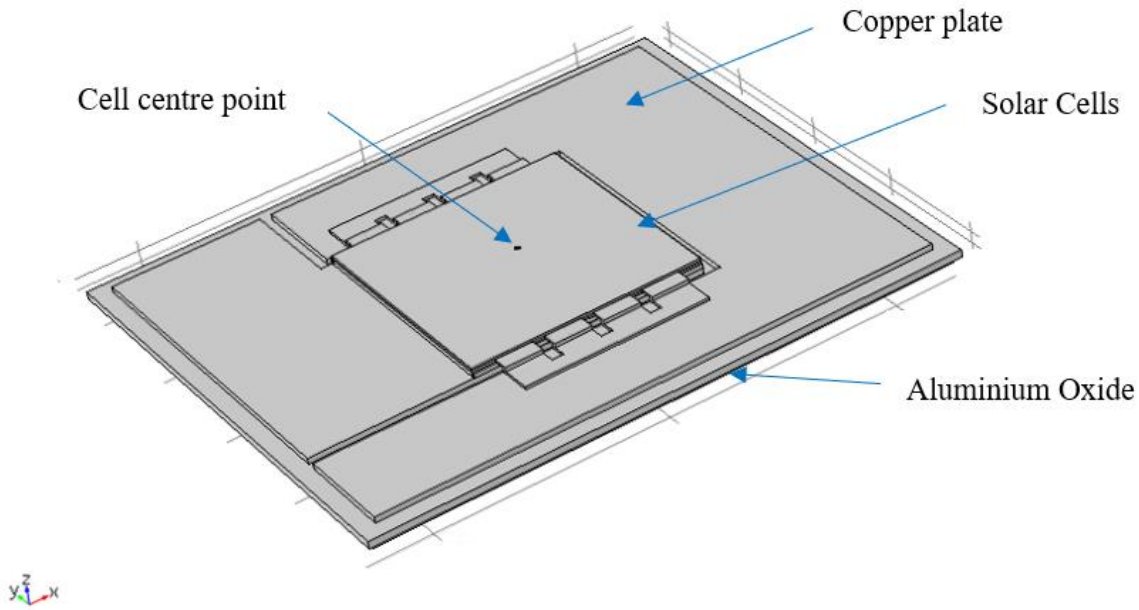

Fig.2. 3D structure of receiver assembly.

4. Results and discussions

4.1. Temperature dependent on cell efficiency

The solar cell generates heat and electrical energy at high optical concentrations. In a series connection, the PV module's efficiency is limited as its temperature increases. A solar receiver assembly usually contains a bypass diode, which will override the cell to avoid overheating, which leads to a reduction in cell/module efficiency (Broderick et al., 2015; Helmers et al., 2013).

The current model accounts for the temperature dependence of the solar cell's efficiency and the effects of temperature from 25-80 ^{o}C and CR= 500x; the trends of efficiency decrease linearly as the temperature increases. The normalised temperature coefficients of the conversion efficiency ($\Delta\eta/dT$) of the triple-junction solar cell is 0.047%/K (Azurspace, 2014). The variation of efficiency with temperature is shown as a linear relationship between temperature and efficiency, as illustrated in Fig.3.

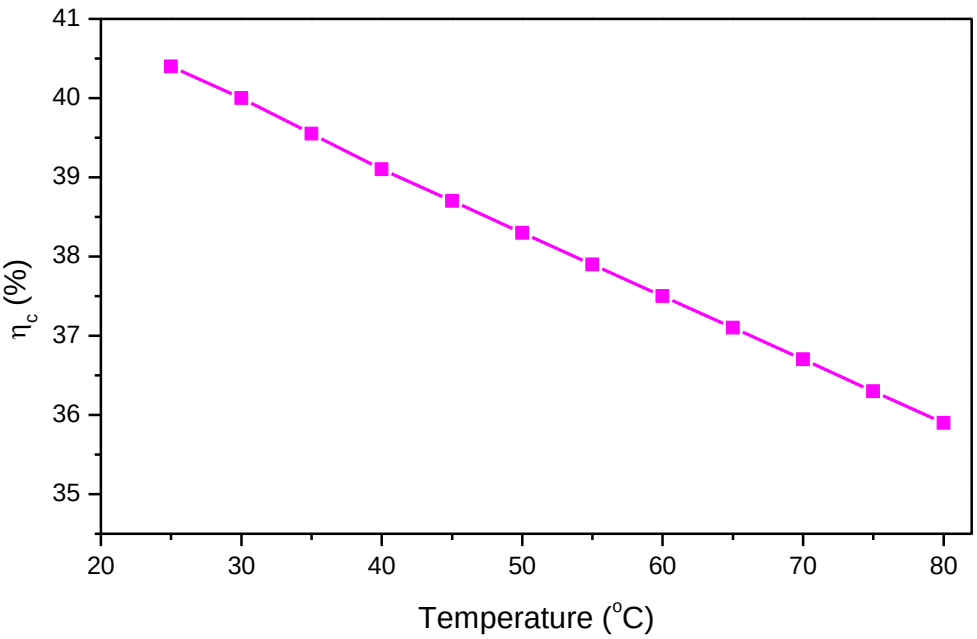

Fig.3. Temperature-dependent on cell efficiency as a function of temperature-dependence from 25-80 ^{o}C and at CR of 500x.

This study considered the transient response to a step input, from unilluminated to being subjected to concentrated (500x) sunlight. During the process of solar concentration, the uniform light of solar radiation is concentrated onto a small area. The thermal gradient is affected by the temperature difference between the edge, and centre, of the solar cell. That is due to the difference in heat dissipation from conduction and convection heat transfer (Cotal and Frost, 2010; Rey-Stolle et al., 2016).

Initially, as the cell temperature rises, the cell material's band gap decreases, hence a larger portion of the incident spectrum can be absorbed by the hottest region. The effect of the temperature rises is a decrease in the operating efficiency of the solar cells. The current mismatch can happen between several regions of a cell operating at different temperatures. The generation of thermal energy at every subcell in GaInP/GaInAs/Ge triple-junction solar cells is higher in the bottom subcell Ge (Sharpe et al., 2013).

4.2. Validation

This proposed model is verified by using data from a commercial PV cell. It is typically used in CPV, the conversion efficiency as a function of temperature from 25-80 ^{o}C versus different values of concentration ratios. Hence, the performance measurement data is presented by AZUR-SPACE Solar Power GmbH, as shown in Fig.4 (Azurspace, 2014). Table 2

summarises a comparison between this study, modelling and measurement at CR = 500x of efficiency at a temperature of 25 ^{o}C. The results show disparities emerging; therefore, the efficiency deviation is about 0.8%, found at 25 ^{o}C, and about 2.5% at a temperature of 80 ^{o}C.

Furthermore, as depicted in Fig.4, as sunlight concentration increases, the efficiencies decrease to a certain level. Hence, the behaviour can be explained by a reduction in series resistance as temperature rises (Ghoneim et al., 2018; Helmers et al., 2013). Moreover, as the FF decreases owing to series losses, the efficiency degendered to a certain level (Fernández et al., 2018).

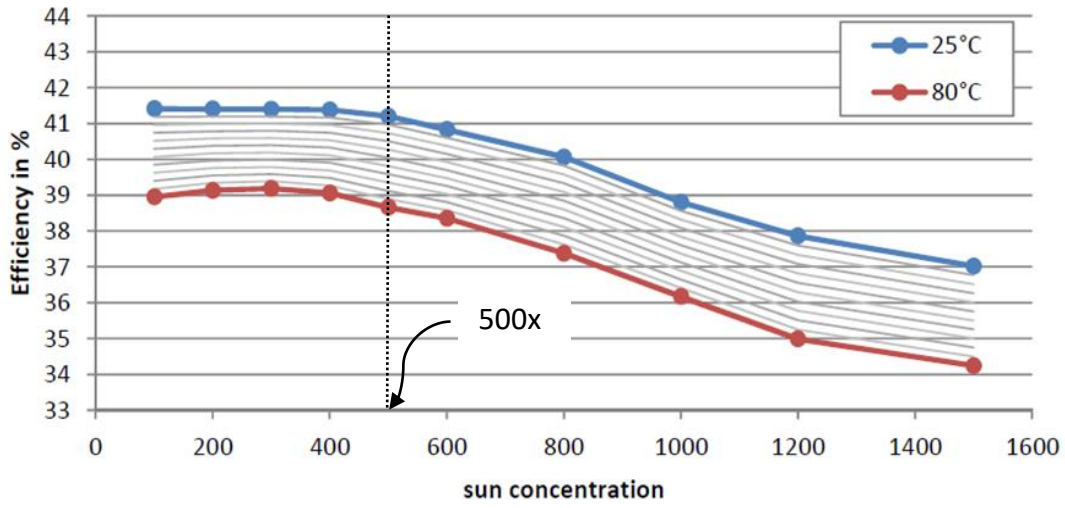

Fig.4. Measured data of performance curve for 3C42A, 2014 by AZUR-SPACE Solar Power GmbH; for concentration ratio from 100 to 1500x versus the conversion efficiency with a variable operating temperature from 25-80 ^{o}C (Azurspace, 2014).

Table 2 Comparison of cell efficiency resulting from this modelling and between experimental data extracted from 3C42A, AZUR-SPACE and current model at 500x.

Temperature (^{o}C)	3C42A η_c (Azurspace, 2014).	Current model η_c	Deviations (%)
25 ^{o}C	41.2%	40.4%	0.8
80 ^{o}C	38.5%	36%	2.5

4.3. Heat power

The main reason for the decrease in cell efficiency at high concentrations is attributed to the temperature rise. The heat power (or heat flux), is the heat generated on the top of the solar cells as a result of optical concentration. The heat power, as a function of temperature, is considered in this study for a temperature range from 25-80 ^{o}C. Under concentration, the heat

power generated by the solar cell is quantified by the given Eq. (11) (Fernández et al., 2014; Ota et al., 2013).

$$q_{heat(T)} = DNI.(1-\eta_c).A_c.CR.\eta_{opt} \quad (11)$$

Temperature-dependence of heat power can be predicted (q_{heat}) based on the efficiency temperature dependence. It indicates that a decrease in heat power due to an efficiency drop increases temperature, as shown in Fig.5. The *DNI* is taken as a constant value of 1000 W/m^2 and *AM* 1.5D; the η_c is variable with cell efficiency as a function of temperature.

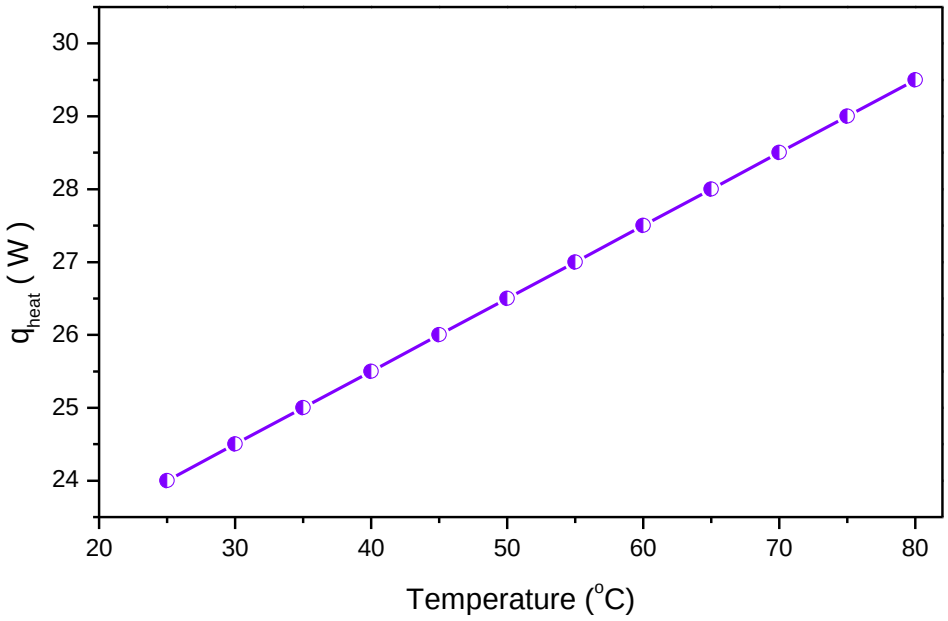

Fig.5. Temperature-dependence on the heat power generated by the cells of temperature from 25-80 °C.

4. 4. Thermal response analysis

In this simulation, the model is run twice: once by using a stationary cell efficiency study, and another by dynamic cell efficiency. The values of dynamic efficiency are variable from 40.4-36%. Thus, the time-dependent model is beneficial in comprehending the heating time required by the cell to reach the steady-state condition. The dynamic model comprises of a series of steady-state models, where the time-step between successive steady-state models becomes a factor.

Based on the FEM model, the initial and boundary conditions are set. As a result, electrical efficiency decreases as a function of temperature, which corresponds to the increase in heat power generated. Therefore, this approach gives an overview of understanding the device's

transient performance. Most of the heat is densely focused in the centre of the solar cell and decreases gradually towards the receiver assembly edge. Fig. 6 shows a graph of steady-state temperature against time, for three values of the timestep, Δt (1,5,10s). Hence, the time-dependent study, where a timestep is set, represents the time differences between each iteration until the end of the computation. As the temperature and corresponding efficiency varies significantly within the larger timesteps, it is clear that the timestep must be maintained at or below 1s to accurately predict the performance of the cell to a step-change in solar flux.

In this model, we consider a uniform illumination on the cell surface. The actual heat dissipation distribution is non-uniform across the receiver. Basically, the heat is transferred through the PV cell's solid layers by conduction. Thus, the heat conduction is most intense at the cell's centre, although, at the edge of the cell, conduction and radiation heat transfer does take place. Eventually, the heat is dissipated to the surrounding environment by convection and radiation heat transfer.

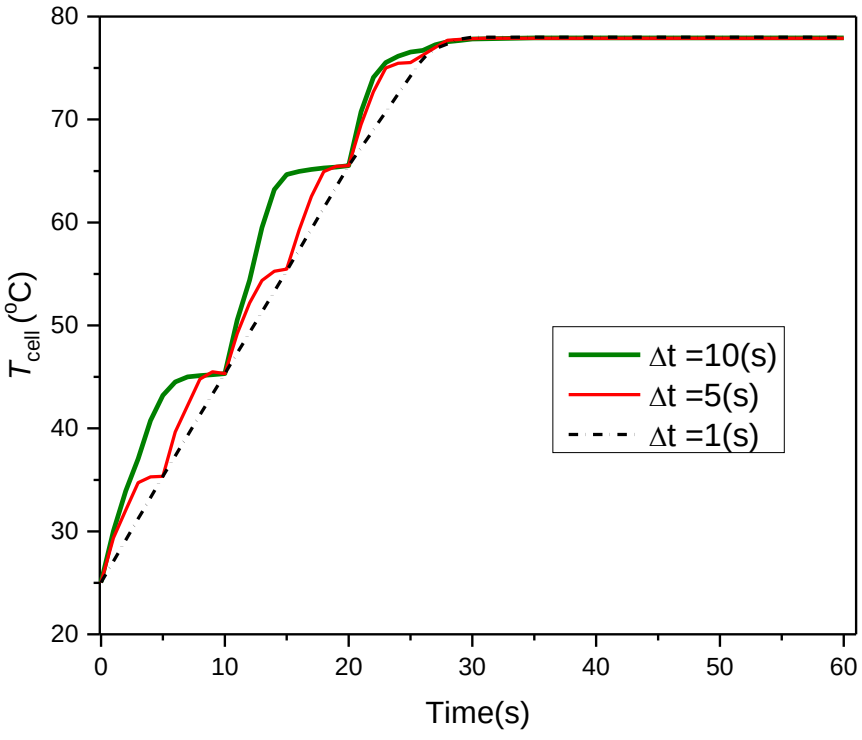

Fig. 6. Transient model results and steady-state temperature against time for three values of the timestep.

The error ratio between the dynamic efficiency with constant efficiency is calculated. Integrated Error (IE) from (0- 60s) is about 12%, from an initial temperature of 25 °C to a

steady-state temperature, which occurred at around 30s; hence, the maximum cell temperature is 78.4 ^{o}C. The Maximum Error Point (MEP) is about 24% and occurs at 10s. In this model, cell temperature loops until reaching a steady-state, although that steady-state occurs when the transient cell temperature (T_{cell}) trends, and adjacent cell temperature, the trend tends to 0%, with a stationery efficiency of 36% and the initial temperature of 25 ^{o}C. Fig.7 shows the results of the comparison between the steady-state temperature for both constant and dynamic efficiency.

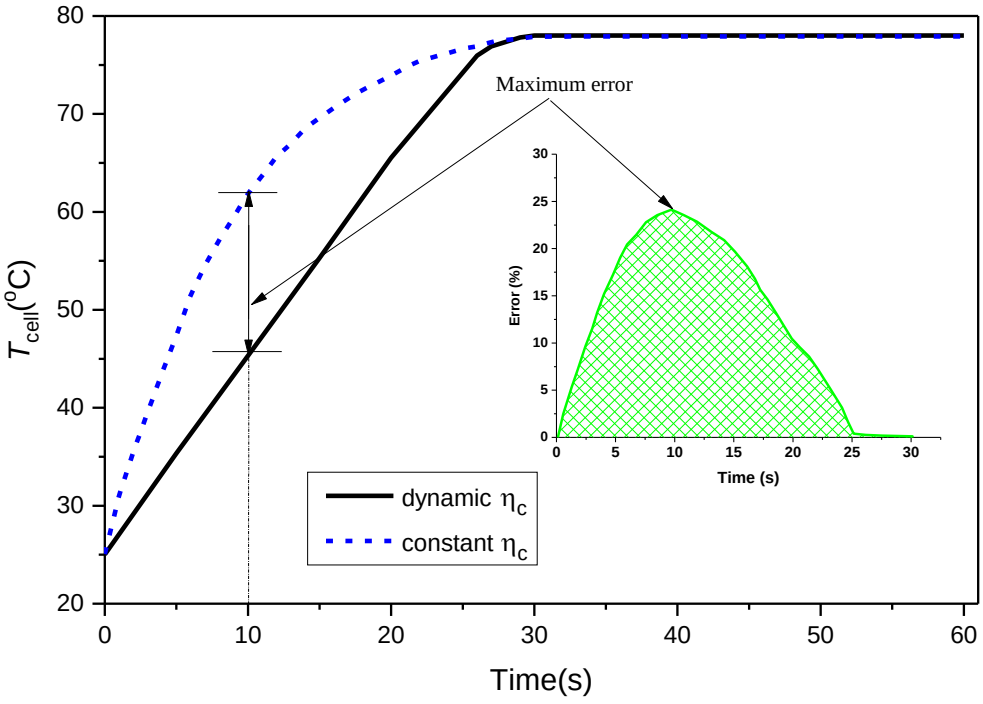

Fig.7. Transient model results in steady-state maximum temperature for both constant efficiency and dynamic efficiency.

The receiver assembly is simulated for time intervals from 0-30s. Fig.8 illustrates the resulting temperature distribution across the cell and receiver assembly for t=0s to t=30s at 5 second intervals (CR = 500x and h_{conv} = 1400 W/m^2 K). The thermal management of the assembly is reliant on convection from the back of the receiver and the environmental conditions. Fig.8 (a) represents the initial cycle simulation when t=0s; hence, the cell temperature is about 25 ^{o}C. In Fig.8. (b), there was a little increase of cell temperature at t=5s, and the maximum cell temperature is shown densely on the centre of the cell and stagnated at 35.5 ^{o}C, but the edge of the cell has the temperature about 28 ^{o}C.

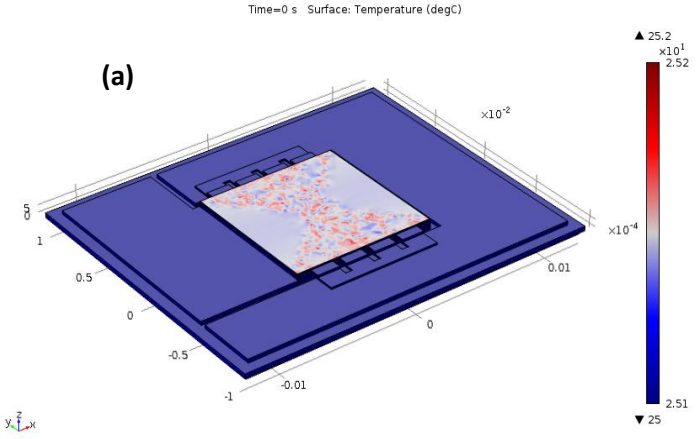

340

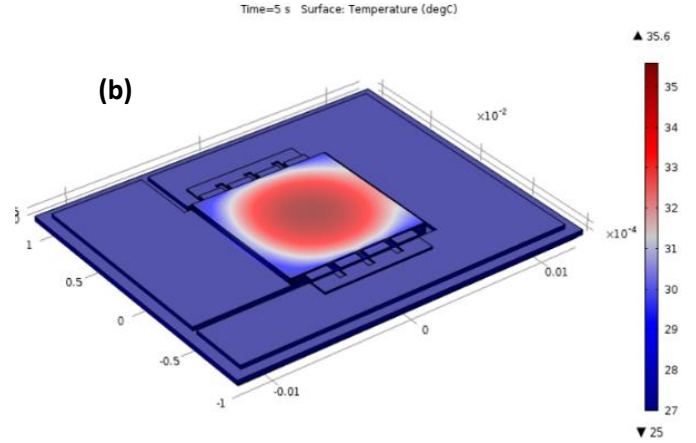

341

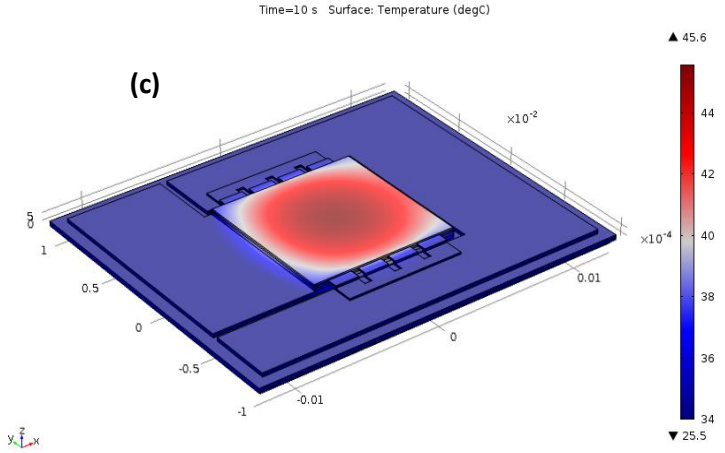

342

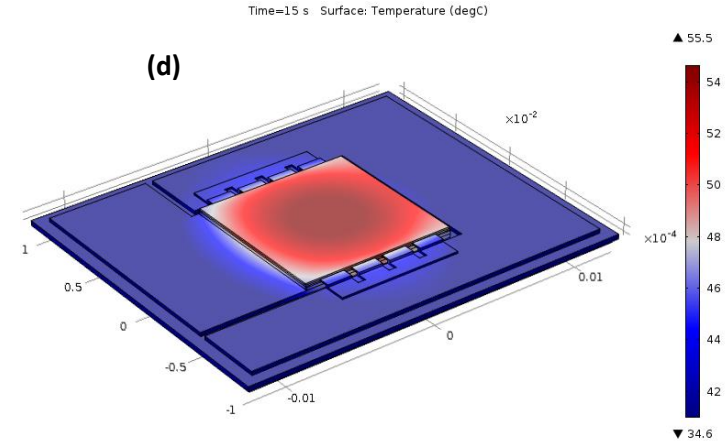

343

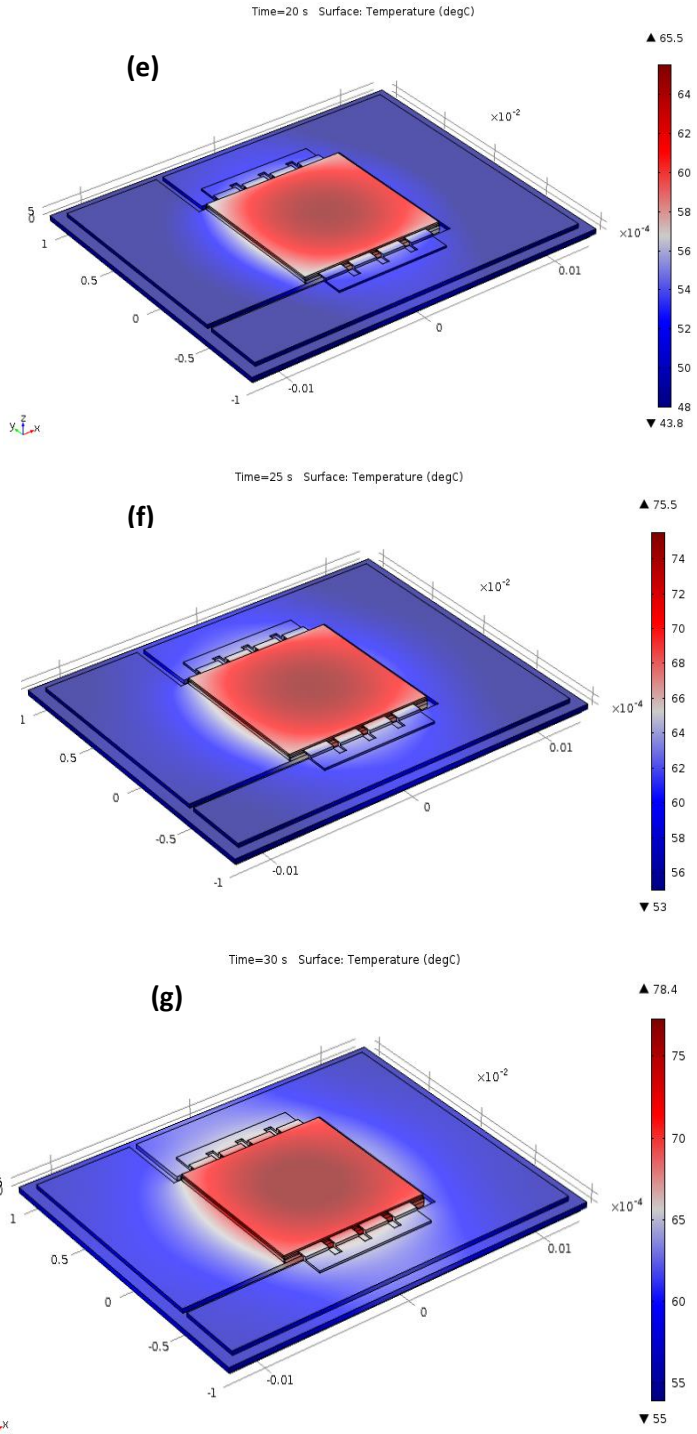

Fig.8. 3D Temperature profile distribution patterns and cell steady-state temperature of the dynamic efficiency of receiver assembly for different intervals as listed in (a, b, c, d, e, f, g) and steady-state time listed respectively (0, 5, 10, 15, 20, 25, 30 seconds).

In Fig.8 (c) the temperature is increased to reach 45.6 ^{o}C at t=10s; temperature distribution pattern on the cell increased at the edge to about 40 ^{o}C. In Fig.8 (d) the temperature of the cell rises to 55.5 ^{o}C at t=15s, and here the temperature of Direct Bonded Copper (DBC) carrier started increasing to reach 34.6 ^{o}C. In Fig.8 (e) the cell temperature increased to reach

65.5 ^{o}C at t=20s, and the (DBC) carrier temperature was about 43.8 ^{o}C. In Fig.8 (f) at t=25s, the cell temperature increased to reach 75.5 ^{o}C, and on the attached (DBC) carrier, the temperature was approximately 53 ^{o}C. Lastly, Fig.8 (g) represents the movement from transient to the steady-state condition at t=30s: the cell temperature was about 74.4 ^{o}C and the pattern temperature distribution on the attached (DBC) carrier, was from 55-65 ^{o}C.

It is cleared that the thermal response of the cell and assembly varies significantly over the 30 second period. Also, if effective and cost-effective thermal management systems are to be designed to optimise the electrical conversion efficiency, and consequently the electrical yield of the system, then dynamic modelling is important (Migliorini et al., 2017).

By comparison, a three-dimensional model (3D) of temperature profile distribution on a multijunction solar cells receiver, presented in Fig. 9, shows results for constant efficiency. For a time period of 0- 60s, the constant efficiency used in this model is approximately 36%, the cell temperature is about 78.4 ^{o}C, and occurs at 30s. The attached (DBC) carrier shows a variable temperature distribution pattern ranging from 55.1-66 ^{o}C. The final maximum cell temperature at dynamic efficiency was similar and therefore reached the steady-state condition at the same time, within 30s, in the constant efficiency.

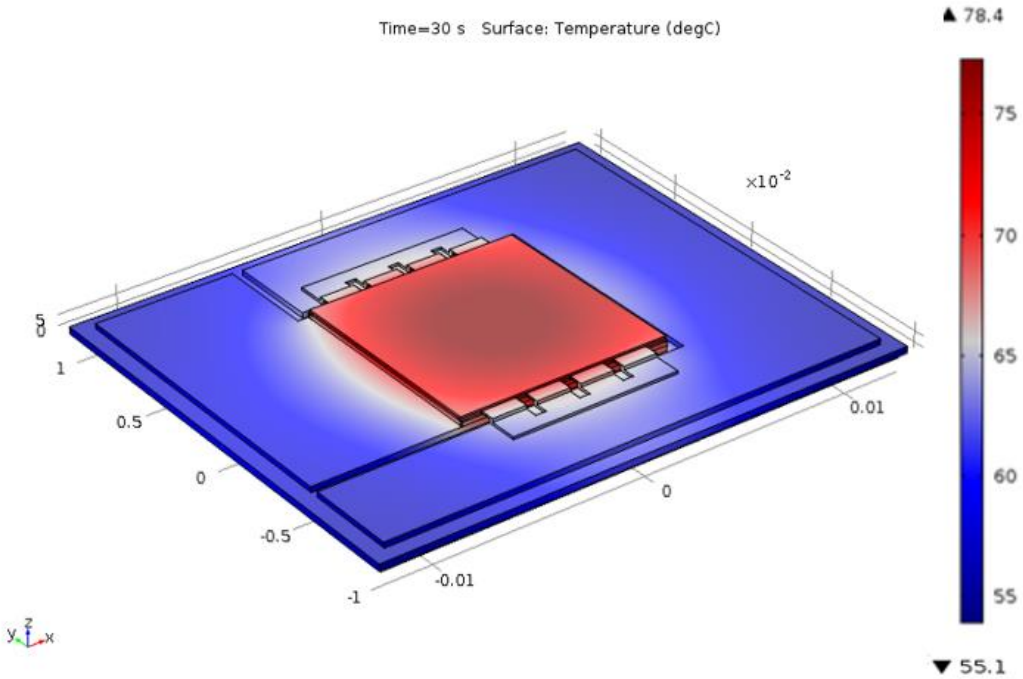

Fig.9. 3D temperature profile distribution, steady-state model at constant efficiency.

In the three-dimensional model, the temperature distribution of the triple-junction cell needs an accurate light profile, since overall input with comprehensive information on a material temperature is dependent on parameters such as energy band gap, absorption, etc. (for semiconductor materials with a stack of multi-junction). Hence, the presence of the 3D model will help in predicting regions of the solar cell, which have malfunctions as an effect of high temperatures (Rey-Stolle et al., 2016).

4.5. Analysis of electrical parameters response

In steady-state conditions, the entire heat generated by the assembly is transferred to the ambient environment. Thus, the optimum thermal management mechanisms reported for CPV application at 500x might include a heat spreader, heat sink, micro-channel, jet impingement and liquid immersion etc. Here, a rear surface convective heat transfer coefficient of 1400 W/m^2 K and an ambient temperature of 25 ^oC was considered, and the predicted cell temperature is approximated to be 78.92 ^oC (Jakhar et al., 2016).

The cell performance is very sensitive to temperature increases, which are simulated in transient methods. In Fig.10, when the solar cell's performance parameters are decreased as temperatures increases, the temperature dependence on the short-circuit current density (J_{sc}) slightly increases over time until the temperature reaches a steady-state at 30s, as shown in Fig. 10 (a). This behaviour can be explained where, as the temperature increases, the energy band gap decreases, as more solar spectrum photon components are absorbed. Subsequently, this leads to a slight increase in short circuit current density.

The temperature dependence on the open circuit's voltage (V_{oc}) decreases over time, as shown in Fig.10 (b). As a result of rising cell temperature, the effects of V_{oc} gradually decreased from 3.01 to 2.84 *V*. The fill factor, also, decreases as cell temperature increases as shown in (Fig.10 (c)). The FF depends on the energy band gap of the cell materials, which is affected more by temperature increases. Therefore, it steadily decreases from 0.84 to 0.78 and stabilises within 30s. The maximum power point also drops as cell temperature increases with time until stagnation temperature stabilises as shown in (Fig.10 (d)). The maximum power (P_{max}) of the cell is gradually decreasing from 19 to 16.7 *W* and reaches a steady-state within 30s.

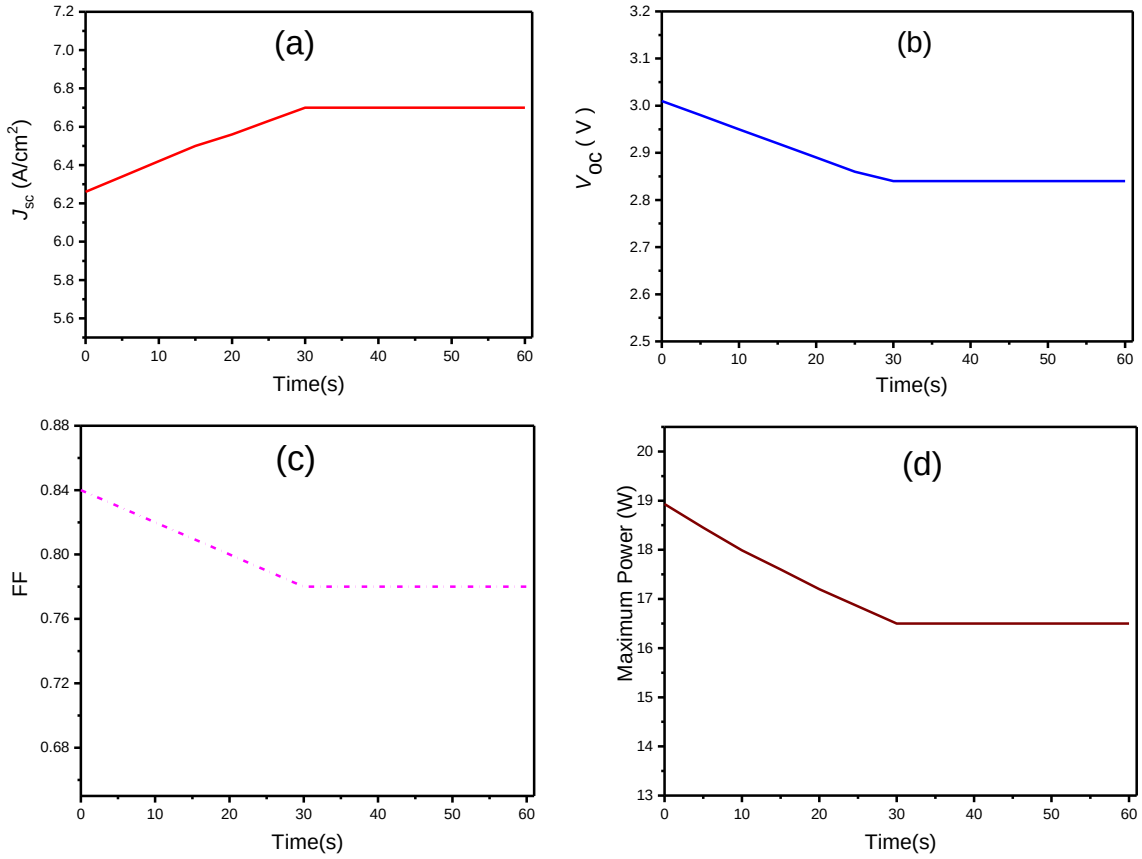

Fig.10. Electrical performance parameters of transient and cell steady-state condition. (a) short current density versus time, (b) open circuit voltage versus time, (c) fill factor versus time, (d) maximum power point versus time intervals.

Fig.11(b) illustrates the overall solar cell's conversion efficiency using the time-dependent temperature, where it tends to decrease towards a steady-state. The efficiency in a time-dependent pattern drops from 40.4% (at 0s) to a steady-state efficiency of about 36.4%, which occurs within 30s. Therefore, this high temperature proves it is the cause of the decrease in the conversion efficiency; the details of that are observed on the process of dynamic losses.

Fig.11(a) represents the power output during the transient and the steady-state condition. As a result of reductions on the parameters of V_{oc}, FF and $P_{amx.}$, when cell temperature rises, the output power also will drop to a certain level. Hence, the shown output power gradually decreases from 18.7 to 16.5 *W* and stabilises within 30s. Based on that, the steady-state output power is fundamental to predicting energy yield gained from the cell/module/system.

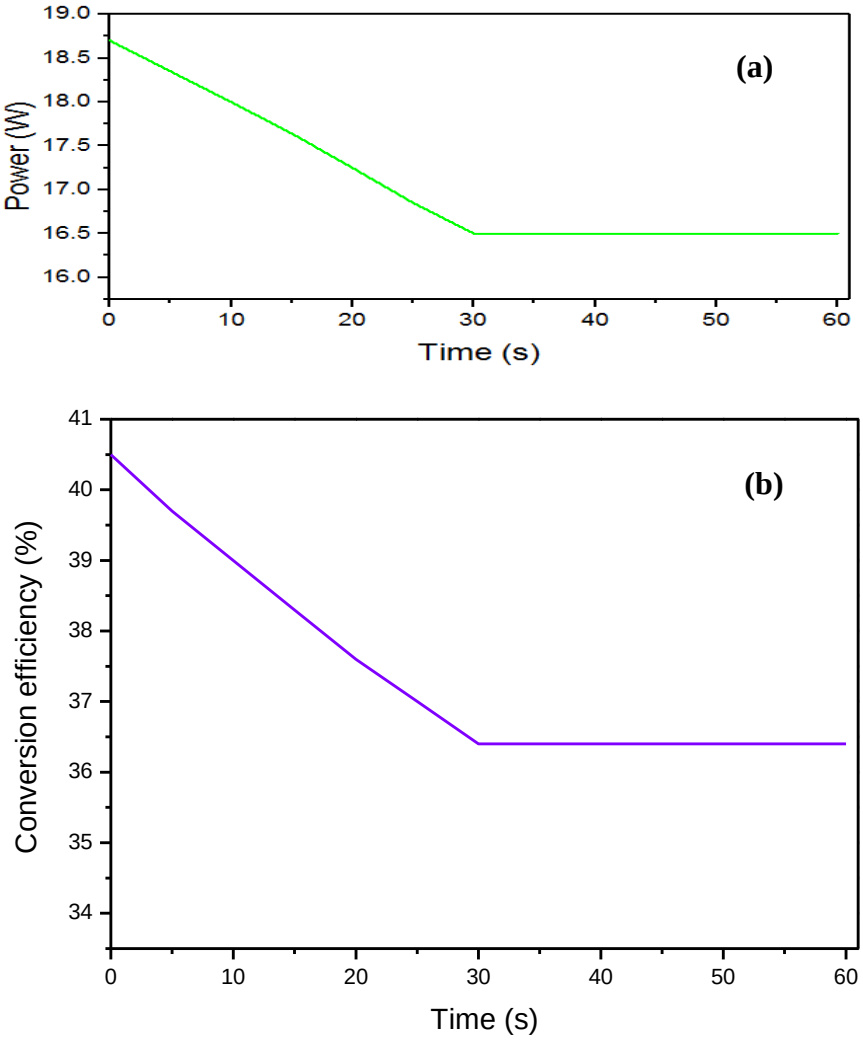

Fig.11. (a) Power output versus transient and steady-state conditions, (b) Conversion efficiency versus cell transient and steady-state conditions.

4.6. Effects of varying irradiance intensity in steady-state cell temperature

Knowing the temperature behaviour of multi-junction solar cells for various irradiations is essential for both the Earth concentrator applications and space applications (Helmers et al., 2013). Despite the impact of temperature on HCPV operating performance and system integrity, the modelling technique used predicts the range of operating temperature for various environmental conditions, including irradiance and environment temperature etc.

The performance of the solar cell is influenced by incident illumination and its operating temperature. Fig.12 depicts the solar cell steady-state temperature versus different values of *DNI*, the optimum time-dependent, selected at Δt =1(s). With the high irradiance intensity of 1000 W/m^2, the steady-state cell temperature was 78.4 ^{o}C at the time of 30s. Hence, at an

irradiance intensity of 700 W/m^2, the steady-state temperature was about 67.5 ^{o}C at the time of 25s. Although, at low values of irradiance intensity of 400 W/m^2, steady-state cell temperature was 56.1 ^{o}C at approximately 20s. This behaviour can be explained, since the slopes of the three case curves are identical, from the initial up to a certain level, as they have a fixed set-up of T_{amb}= 25 ^{o}C and h_{conv} =1400 W/m^2 K. On the other hand, the achieved values of steady-state cell temperature are different here, due to the various values of the *DNI* and corresponding *AM*.

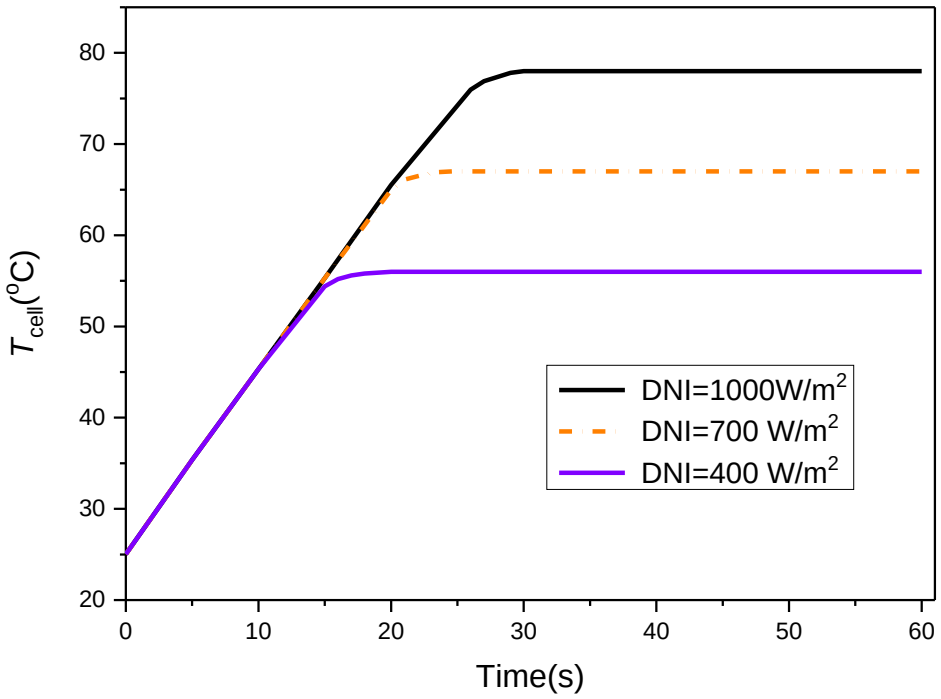

Fig.12. Effects of changes *DNI* in the cell temperature at dynamic efficiency for time for steady-state temperature.

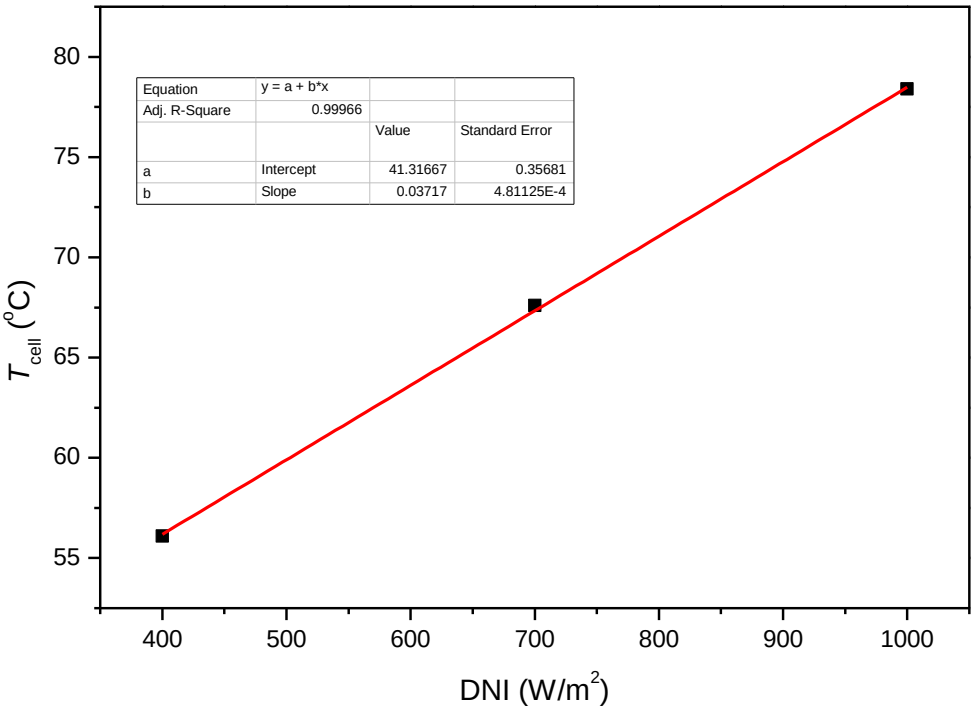

Fig.13. Different values of *DNI* versus cell temperature at steady-state temperatures.

The irradiance intensity has a significant influence on steady-state cell temperature. As the values of *DNI* changes at conditions of (1000 W/m^2, 700 W/m^2, 400 W/m^2) the slope linearly increases; the regression was (R^2 = 0.9996). The predicted cell temperature was variable (between 78.4 - 56.1 ^{o}C), the cell efficiency decreased sharply from 36.4% to 32.3%, as illustrated in Fig.13. The cell steady-state temperature response remarkably shows the effect of increases and decreases of *DNI* at the steady-state cell temperature. It's important here to mention that 1000 W/m^2 of the *DNI* and corresponding *AM* represents the midday operating condition, which is approximately the maximum values during the operation. In contrast, 400 W/m^2 of the *DNI* and corresponding *AM* represents the period of sunrise/sunset, which are the lowest values.

Table 3 Detailed variation of *DNI* for maximum cell temperature, steady-state conversion efficiency and time.

Parameters	*DNI* =1000 (W/m^2)	*DNI* =700 (W/m^2)	*DNI* = 400 (W/m^2)
Steady-state T_{cell} (^{o} C)	78.4	67.5	56.1
Steady-state (η_c)	36.4	34.5	32
Steady-state time (s)	30	25	20

In summary, as shown, the increase of *DNI* leads to an increase in cell temperature as a result of increased heat flux and a reduction in conversion efficiency. Table 3 also summarised the comparison of different *DNI* steady-states values. Nonetheless, to be considered on a daily basis, the *DNI* values are variable between sunrise, midday and sunset; the cell's operating performance behaviour will change accordingly.

Fig.14 illustrates the different values of *DNI* and their corresponding values of *AM.* As is significantly shown in Fig.14, there is a directly proportional relationship between these two parameters. The *AM* is a measure of the atmospheric depth crossed by solar radiation. Also, the *AM* had significant effects on the wavelengths of solar radiation. In the real operating conditions daily, the values of *AM* and *DNI* are variable, from sunrise to sunset, and will be considered in future work.

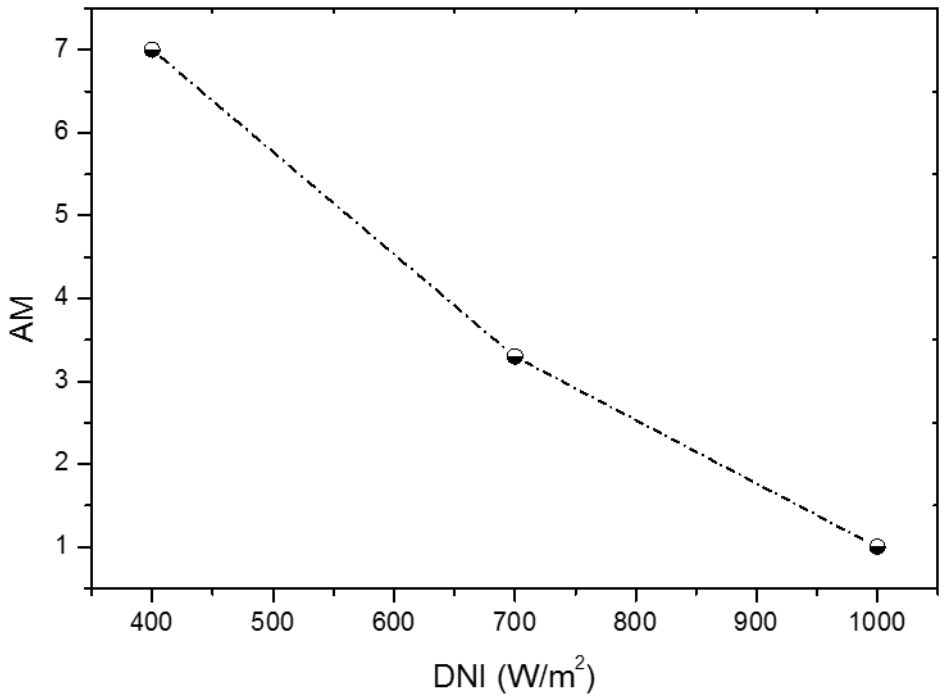

Fig.14. Different values of *DNI* various the corresponding values of *AM*.

4.7. Effects of varying ambient temperature in the steady-state cell temperature

The factor which is essential when considering the PV cell temperature is the ambient temperature, with regards to the variability of ambient temperature and its effect on the solar cell's steady-state temperature. In this scenario, when the *DNI* = 1000 W/m^2 and the ambient temperature T_{amb} = 25 ^{o}C, the steady-state cell temperature is 78.4 ^{o}C for h_{conv} =1400 W/m^2

K. Furthermore, for T_{amb} = 35 °C, the steady-state cell temperature is about 78.8 °C and the response of h_{conv} = 1500 W/m^2. For T_{amb} = 45 °C, the steady-state cell temperature is about 79.2 °C and the response of h_{conv} = 1600 W/m^2 K. Fig.15 illustrates the steady-state cell temperature at a variety of ambient temperatures. This behaviour can be explained by the higher heat transfer coefficient leading to lower thermal resistance, which in turn lowers the operating temperature of the CPV cell/module.

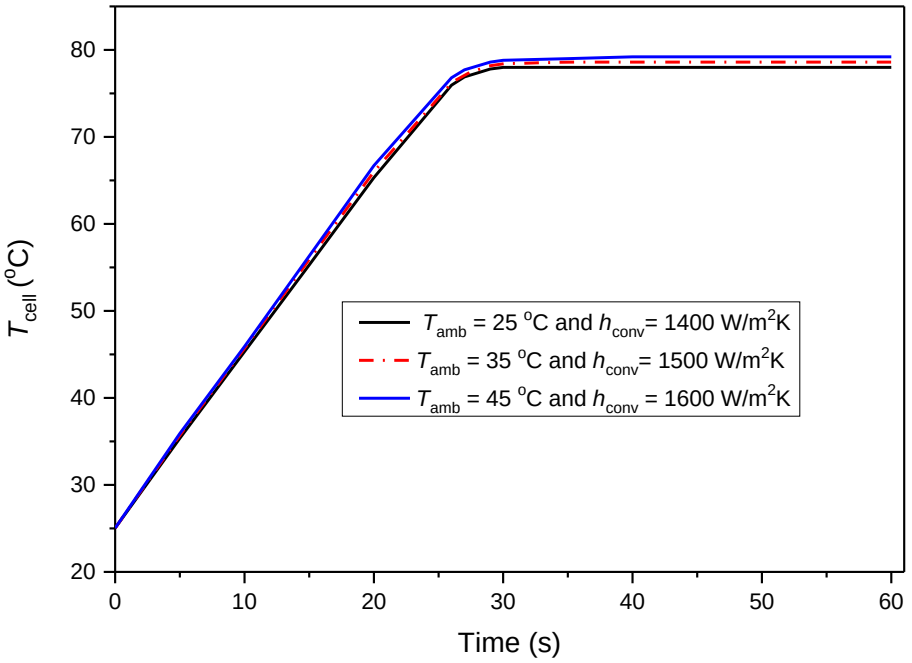

Fig.15. Effects of different ambient temperature on the steady-state cell temperature in order to maintain the temperature below a safe level and the response of convection heat transfer coefficient.

The predicted model can provide monitoring of the devices in order to have a better understanding of performance behaviour, which will enable proper selection of appropriate solutions for heat dissipation. Hence, transient analysis of the thermal and electrical behaviour is performed, and these collected notifications will be used to provide improved knowledge of CPV performance behaviour. The techniques to limit the influence of the operating temperature of the internal device are not assessed; it needs more advanced tools for accurate prediction.

5. Conclusions

In this work, a model was developed to characterise the transient thermal and electrical performance of triple-junction solar cells. The transient model here is used to comprehend the transient state during operating conditions. Consequently, it is significant to our understanding of operating performance behaviour, and it is a step towards enhancing the device design. The conclusions of this work are summarised below as follows:

- It has been established that a time step, Δt of 1s is required for the range of parameters studied, to accurately predict cell performance. Through the dynamic model, the impact of different incident solar flux values on the power output of the photovoltaic device could also be determined. A dynamic efficiency compared with constant efficiency, and integrated error is about 12%.
- The comparison of the cell temperatures ranging from 25-80 ^{o}C is reported. The difference in the efficiency of approximately 0.8% is found for lower temperatures, and this rises to approximately 2.5% for the higher temperatures within the range considered.
- Cell steady-state temperature occurs at a maximum cell temperature of 78.4 ^{o}C within the 30s, at convective heat transfer coefficient h_{conv}=1400 W/m^2 K and concentration ratio CR= 500x. Furthermore, in scenario of T_{amb} = 35 ^{o}C, the steady-state cell temperature is about 78.8 ^{o}C and the thermal response of h_{conv} = 1500 W/m^2. For T_{amb} = 45 ^{o}C, the steady-state cell temperature is about 79.2 ^{o}C and the thermal response of h_{conv} = 1600 W/m^2 K. Thus, as deduced at high ambient temperature, there will be a requirement for high convective heat transfer coefficients to maintain a cell operating temperature below 80 ^{o}C.
- The higher value of *DNI* 1000 W/m^2 and the corresponding lower value of *AM* represents the midday operating condition, which is approximately the maximum values during the operation. The steady-state cell temperature was 78.4 ^{o}C at the time of 30s. In contrast, lower values of *DNI* 400 W/m^2 and the corresponding higher value of *AM* represents the period of sunrise/sunset, which are the lowest values. The steady-state cell temperature was 56.1 ^{o}C at approximately 20s.
- The present study contributes to the understanding of the transient state, that lies in the link between the ideal modelling and environmental operating conditions.

Consequently, that is very significant in our comprehension of the transient nature of CPV receivers.

Based on the approaches mentioned above and outcomes, in the future, it is recommended that research studies include dynamic performance measuring/modelling for both small and large-scale operations with consideration to the weather and environmental data.

Acknowledgement

Many grateful thanks to the School of Engineering and Physical Sciences, Heriot-Watt University, United Kingdom, also many thanks to Libyan Authority for Research Science and Technology.

References

AEO, 2019. Annual Energy Outlook with projections to 2050,. January 24, 2019 www.eia.gov/aeo.

Aldossary, A., Mahmoud, S., Al-Dadah, R., 2016. Technical feasibility study of passive and active cooling for concentrator PV in harsh environment. Appl. Therm. Eng.100, 490-500.

Araki, K., Uozumi, H., Yamaguchi, M., 2002. A simple passive cooling structure and its heat analysis for 500/spl times/concentrator PV module, Photovoltaic Specialists Conference, 2002. Conference Record of the Twenty-Ninth IEEE. IEEE, pp. 1568-1571.

Azurspace, 2014. triple junction solar cell assembly – Type 3C42A. data sheet.

Broderick, L.Z., Albert, B.R., Pearson, B.S., Kimerling, L.C., Michel, J., Cells, S., 2015. Design for energy: Modeling of spectrum, temperature and device structure dependences of solar cell energy production. Sol. Ener. Mater. Sol. Cells. 136, 48-63.

Cengel, Y.A., 1998. Heat transfer: a practical approach. WBC McGraw-Hill.

Ceylan, İ., Gürel, A.E., Ergün, A., Tabak, A., 2016. Performance analysis of a concentrated photovoltaic and thermal system. Sol. Energy 129, 217-223.

Cotal, H., Fetzer, C., Boisvert, J., Kinsey, G., King, R., Hebert, P., Yoon, H., Karam, N., 2009. III–V multijunction solar cells for concentrating photovoltaics. Ener. & Enviro. Sci. 2(2), 174-192.

Cotal, H., Frost, J., 2010. Heat transfer modeling of concentrator multijunction solar cell assemblies using finite difference techniques, Photovoltaic Specialists Conference (PVSC), 2010 35th IEEE. IEEE, pp. 000213-000218.

Cotal, H., Sherif, R., 2006. Temperature dependence of the IV parameters from triple junction GaInP/InGaAs/Ge concentrator solar cells, Photovoltaic Energy Conversion, Conference Record of the 2006 IEEE 4th World Conference on. IEEE, pp. 845-848.

Council, W.E., 2016. World energy resources 2016. World Energy Council, London, UK.

Fernández, E.F., Almonacid, F., Rodrigo, P.M., Pérez-Higueras, P.J., 2018. CPV systems, McEvoy's Handbook of Photovoltaics. Elsevier, pp. 931-985.

Fernández, E.F., Rodrigo, P., Almonacid, F., Pérez-Higueras, P., 2014. A method for estimating cell temperature at the maximum power point of a HCPV module under actual operating conditions. Sol. Ener. Mater. Sol. Cells. 124, 159-165.

García, I., Victoria, M., Antón, I., 2016. Temperature effects on CPV solar cells, optics and modules. Handbook on Concentrator Photovoltaic Technology, 245.

Geisz, J.F., Steiner, M.A., Jain, N., Schulte, K.L., France, R.M., McMahon, W.E., Perl, E.E., Friedman, D.J.J.I.J.o.P., 2017. Building a six-junction inverted metamorphic concentrator solar cell. IEEE Journal of Photovoltaics 8(2), 626-632.

Ghoneim, A.A., Kandil, K.M., Alzanki, T.H., Alenezi, M., 2018. Performance analysis of high-concentrated multi-junction solar cells in hot climate. International Journ. Sustain. Energy 37(3), 294-310.

Green, M.A., Dunlop, E.D., Levi, D.H., Hohl-Ebinger, J., Yoshita, M., Ho-Baillie, A.W, applications, 2019. Solar cell efficiency tables (version 54). 27(7), 565-575.
Helmers, H., Schachtner, M., Bett, A.W., Cells, S., 2013. Influence of temperature and irradiance on triple-junction solar subcells. Sol. Energ. Mater. Sol. Cells. 116, 144-152.
Jakhar, S., Soni, M., Gakkhar, N., 2016. Historical and recent development of concentrating photovoltaic cooling technologies. Renew. Sustain. Energy Rev.. 60, 41-59.
Kinsey, G.S., Edmondson, K.M., 2009. Spectral response and energy output of concentrator multijunction solar cells. Progress in Photovoltaics: Research and Applications 17(5), 279-288.
Kumar, N.S., Matty, K., Rita, E., Simon, W., Ortrun, A., Alex, C., Roland, W., Tim, G., Kumar, M.T., 2012. Experimental validation of a heat transfer model for concentrating photovoltaic system. Appl.Therm. Eng. 33, 175-182.
Maka, A.O., O'Donovan, T.S., 2020. A review of thermal load and performance characterisation of a high concentrating photovoltaic (HCPV) solar receiver assembly. Sol. Energy 206, 35-51.
Maka, A.O., O'Donovan, T.S., 2019a. Analysis of thermal response and electrical characterisation of triple-junction solar cells based on variable solar spectral irradiance and air mass. Therm. Sci. Eng. Prog. 10, 269-279.
Maka, A.O., O'Donovan, T.S., 2019b. Modelling of the thermal behaviour of solar high concentrating photovoltaic receiver. Therm. Sci. Eng. Prog. 9, 281-288.
Migliorini, L., Molinaroli, L., Simonetti, R., Manzolini, G., 2017. Development and experimental validation of a comprehensive thermoelectric dynamic model of photovoltaic modules. Sol. Energy 144, 489-501.
Muller, M., Kurtz, S., Steiner, M., Siefer, G., 2015. Translating outdoor CPV I–V measurements to a CSTC power rating and the associated uncertainty. Prog. in photovoltaics: Research and Applications 23(11), 1557-1571.
Multiphysics, C., 2012. COMSOL multiphysics user guide (Version 4.3 a). COMSOL, AB, 39-40.
Muron, A., Chow, S., Wheeldon, J., Hinzer, K., Schriemer, H., 2011. Thermal optimization of a solar cell carrier for concentrator systems, Photonics North 2011. International Society for Optics and Photonics, p. 800722.
Nishioka, K., Sueto, T., Uchida, M., Ota, Y., 2010. Detailed analysis of temperature characteristics of an InGaP/InGaAs/Ge triple-junction solar cell. Journal of electronic materials 39(6), 704-708.
Ota, Y., Nagai, H., Araki, K., Nishioka, K., 2013. Thermal transfer simulation for concentrator photovoltaic receiver under concentration condition, 9TH INTERNATIONAL CONFERENCE ON CONCENTRATOR PHOTOVOLTAIC SYSTEMS: CPV-9. AIP Publishing, pp. 18-21.
Peharz, G., Siefer, G., Bett, A., 2009. A simple method for quantifying spectral impacts on multi-junction solar cells. Sol. Energy 83(9), 1588-1598.
Philipps, S.P., Bett, A.W., Horowitz, K., Kurtz, S., 2015. Current status of concentrator photovoltaic (CPV) technology. National Renewable Energy Lab.(NREL), Golden, CO (United States).
Philipps, S.P., Bett, A.W.J., 2014. III-V Multi-junction solar cells and concentrating photovoltaic (CPV) systems. Advan. Opt. Technolog. 3(5-6), 469-478.
REGR, 2018 Renewables Energy Global status Report - REN21,. www.ren21.net/wp-content/.../2018/06/17-8652_GSR2018_FullReport_web_final_.pdf.
Rey-Stolle, I., Olson, J.M., Algora, C., 2016. Concentrator Multijunction Solar Cells. Handbook on Concentrator Photovoltaic Technology, 59.
Sarhaddi, F., Farahat, S., Ajam, H., Behzadmehr, A., Adeli, M.M., 2010. An improved thermal and electrical model for a solar photovoltaic thermal (PV/T) air collector. Appl. Energy 87(7), 2328-2339.
Sharpe, A., Eames, P., Dimroth, F., Araki, K., Antón, I., 2013. Modelling of multijunction cell temperature distributions subject to realistic operating conditions, AIP Conference Proceedings. AIP, pp. 142-146.
Sweet, T.K.N., Rolley, M.H., Li, W., Paul, M.C., Johnson, A., Davies, J.I., Tuley, R., Simpson, K., Almonacid, F.M., Fernández, E.F., 2018. Design and characterization of hybrid III–V concentrator photovoltaic–thermoelectric receivers under primary and secondary optical elements. Appl. Energy 226, 772-783.

630 Talavera, D., Pérez-Higueras, P., Ruíz-Arias, J., Fernández, E., 2015. Levelised cost of electricity in
631 high concentrated photovoltaic grid connected systems: spatial analysis of Spain. Appl. Energy
632 151, 49-59.
633 Theristis, M., O'Donovan, T.S., 2015. Electrical-thermal analysis of III–V triple-junction solar cells
634 under variable spectra and ambient temperatures. Sol. Energy 118, 533-546.
635 Theristis, M., Sarmah, N., Mallick, T.K., O'Donovan, T.S., 2012. Design and numerical analysis of
636 enhanced cooling techniques for a high concentration photovoltaic (HCPV) system, 27th
637 European Photovoltaic Solar Energy Conference and Exhibition. pp. 260-265.
638 Torres-Lobera, D., Valkealahti, S., 2014. Inclusive dynamic thermal and electric simulation model of
639 solar PV systems under varying atmospheric conditions. Sol. Energy 105, 632-647.
640 Wang, N.-Y., Chiang, S.-Y., Chou, T.-L., Shih, Z.-H., Hong, H.-F., Chiang, K.-N., 2010. Transient
641 thermal analysis of high-concentration photovoltaic cell module subjected to coupled thermal
642 and power cycling test conditions, Thermal and Thermomechanical Phenomena in Electronic
643 Systems (ITherm), 2010 12th IEEE Intersociety Conference on. IEEE, pp. 1-6.
644 Watts, R.G., 2013. Engineering response to climate change. CRC Press.
645 Zhangbo, Y., Qifen, L., Qunzhi, Z., Weiguo, P., 2009. The cooling technology of solar cells under
646 concentrated system, Power Electronics and Motion Control Conference, 2009. IPEMC'09.
647 IEEE 6th International. IEEE, pp. 2193-2197.